Adv. Polar Upper Atmos. Res., 16, 84–98, 2002


# *E* region echoes observed with the Syowa HF radar under disturbed geomagnetic conditions

Tadahiko Ogawa[1], Nozomu Nishitani[1], Natsuo Sato[2], Hisao Yamagishi[2] and Akira Sessai Yukimatu[2]

[1]*Solar-Terrestrial Environment Laboratory, Nagoya University, Honohara, Toyokawa 442-8507*
[2]*National Institute of Polar Research, Kaga 1-chome, Itabashi-ku, Tokyo 173-8515*

***Abstract***: *E* region radar echo parameters (echo power, Doppler velocity and spectral width) obtained with the Syowa Station HF radar under disturbed geomagnetic conditions are qualitatively analyzed to study how echoing region changes due to HF wave refraction caused by ionospheric disturbance. It is found that with increasing disturbance level, echo ranges become shorter because of wave refraction during propagation due to more enhanced *D* and *E* region electron density. When geomagnetic *H* component variation ($\Delta H$) is less than about $-900$ nT, echoes are returned from the central *E* region where geomagnetic aspect angle is close to zero. When $\Delta H$ is very high ($\simeq -1500$ nT), the echoes are backscattered from the *D* and lower *E* regions and their power, Doppler velocity and spectral width are largely suppressed. The results suggest that we must always consider, more or less, wave refraction effect in analyzing near-range *E* region HF radar echoes.

## 1. Introduction

The Super Dual Auroral Radar Network (SuperDARN) HF radars can detect coherent echoes backscattered by field-aligned irregularities at slant ranges from 180 to 3000 km (or more), that is, at altitudes including the ionospheric *D*, *E* and *F* regions (Greenwald *et al.*, 1995). A Japanese Antarctic station, Syowa Station (69.0°S, 39.6°E; magnetic latitude 66.2°S; *L*-value=6.1), has been operating two SuperDARN radars, called the "Syowa South" and "Syowa East" radars. *E* region echoes detected with these radars have been analyzed in detail by Koustov *et al.* (2001) and Makarevitch *et al.* (2001, 2002) who used simultaneous data from a VHF auroral radar at Syowa Station. They compared Doppler velocity and echo power from the HF radars with those from the VHF radar to discuss similarity and dissimilarity between both radar echoes. One of the findings is that HF wave refraction during propagation must be considered in explaining HF echo characteristics (Villain *et al.*, 1984; Uspensky *et al.*, 1994). *E* region echoes at northern high latitudes have been studied by, for example, Uspensky *et al.* (2001) who also pointed out the important role of ionospheric refraction.

Ogawa *et al.* (2001) have used a large data-set of Doppler velocity obtained for 11 months in 1997 with the Syowa East radar under various geomagnetic conditions to discuss statistical characteristics of the velocity at slant ranges of 180–1200 km and their implications. They found that on average the velocity has a minimum of about 100 m/s at 180–225

km ranges and that it increases monotonically with range to attain a maximum of 300–350 m/s at 400–500 km. Such a range profile is caused by the combined effects of altitude-dependent phase velocities of ionospheric plasma waves and HF wave refraction, and partly by meteor winds. Ogawa *et al.* (2001) speculated that the low velocity (~100 m/s) at ranges of 180–225 km may originate in part from neutral winds and/or turbulence of the neutral atmosphere. Ogawa *et al.* (2002) have found that polar mesosphere summer echoes are another candidate for the low velocity at ranges of 180–315 km. However, other possible reasons to explain the low velocity at short ranges have not been explored.

Refraction of an HF radar wave becomes more severe with increasing electron density in the $D$ and $E$ regions. The density is enhanced during disturbed geomagnetic conditions (*e.g.*, Miyazaki *et al.*, 1981), thus suggesting that HF-scattering area and altitude change depending on geomagnetic disturbance level. Such change has been never considered, in quantitative manner, in the previous $E$ region HF echo studies that pointed out refraction effect. This paper is concerned with $E$ region echoes detected with the Syowa East radar under weakly, strongly and very strongly disturbed geomagnetic conditions, and aims to show qualitatively how the echo region shifts toward the radar due to wave refraction under disturbed conditions.

## 2. Syowa East radar

Figure 1 displays field of view (FOV) of the Syowa East radar in geographic coordinates. The FOV is covered with 16 narrow beams (beam numbers 0, 1, 2, ..., 15) over an azimuth sector of 52°. Each beam width is believed to be around ~4.5° for the radar frequencies (10.2–12.2 MHz) used in our observations (Greenwald *et al.*, 1985). The beam direction of beam 0 is almost perpendicular (80°) to the magnetic $L$-shells and that of beam 15 has an angle of 20° to them. The radar beam in the normal SuperDARN operation is sequentially scanned from beam 0 to beam 15 (16 azimuth bearings) with a step in azimuth of 3.3°, a scan repeat time of ~120 s, a range resolution of 45 km, and a peak power of around 10 kW. The first range gate is set to 180 km.

Figure 1 also depicts contour lines (solid curves) of the angle ($A$) between the radar wave vector and the geomagnetic field vector (IGRF95) at an altitude of 110 km around which auroral electrojet intensity is strongest and $E$ region irregularities are most enhanced (*e.g.*, Ogawa *et al.*, 1976). Note that the geomagnetic aspect angle $\alpha$ is defined as $90^\circ - A$. It is well known that coherent radar echoes are strongly backscattered from an area where $A$ is between between 89° and 91° and that the strongest backscatter occurs at $A = 90^\circ$. Figure 1 indicates that such area is located at ground range of around 275 km (slant range of 290 km) on beam 0 and of around 500 km (slant range of 508 km) on beam 15. Previous VHF (50 MHz) radar observations at Syowa Station indicated that echoes on a radar beam nearly perpendicular to the $L$-shells are strongest at a range of around 280 km (Ogawa and Igarashi, 1982; Ogawa *et al.*, 1989; Koustov *et al.*, 2001). Note that no radar wave refraction during propagation is assumed in the calculations. This assumption is almost valid for VHF waves but not always valid for the SuperDARN HF waves (8–15 MHz) because of possible wave refraction due to enhanced electron density (Villain *et al.*, 1984).

The aspect angle ($\alpha$) distribution shown in Fig. 1 varies depending on altitude.

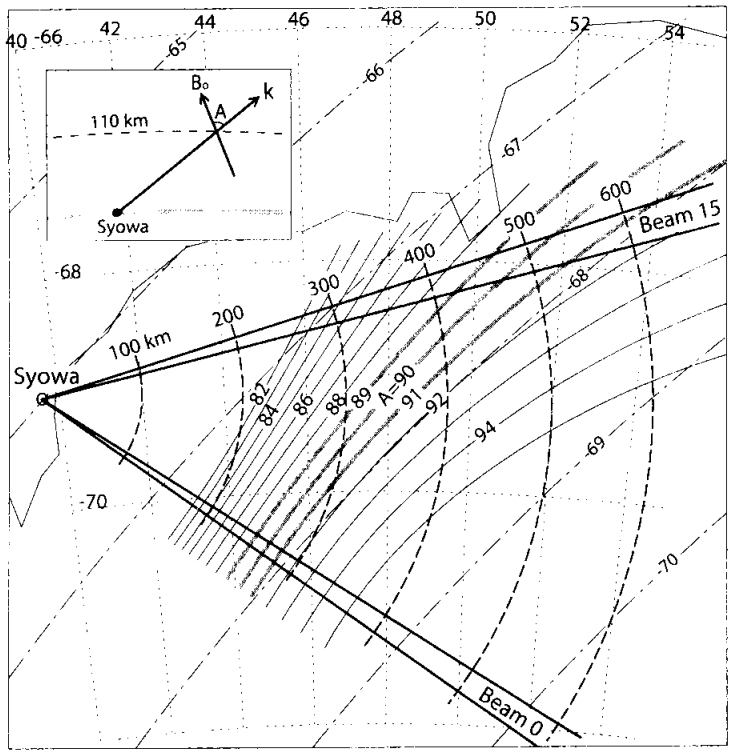


*Fig. 1. Field of view of the Syowa East HF radar covered with 16 narrow beams (beam numbers 0, 1, 2, ..., 15) in geographic coordinates. Ground ranges (100 km step) from Syowa Station are marked by the dashed curves. Contour lines of angle (A) between radar wave and the geomagnetic field vectors at an altitude of 110 km are shown by the solid curves. Geomagnetic latitudes are shown by the dot-dashed curves.*

Figure 2 plots some ray paths (elevation angles of 4°-30°) from the Syowa radar in altitude-ground range coordinates (Ogawa *et al.*, 2001). The area having $\alpha$ between $-1°$ and $+1°$ is surrounded by the thick solid curves. On beam 0 (Fig. 2a) the radar waves with elevation angles of 20°-23° are backscattered from altitudes of 100-120 km at slant ranges of 250-320 km, while on beam 15 (Fig. 2b) these values are 7°-13° and 400-650 km. The path length crossing the $E$ region altitude becomes longer with increasing beam number.

Radar echo intensity depends on echo range, cross-section of a target, radar antenna pattern and so on. The vertical pattern of the SuperDARN antenna array is quite broad with an average half power beamwidth of ~30°, and at 8 MHz the sensitivity maximizes at an elevation angle of 35° whereas at 20 MHz this value decreases to 15° (Greenwald *et al.*, 1985): the sensitivity at angles larger than 60° is believed to be very low. This means that the Syowa HF antenna has a maximum gain at around 28°-30° at 10-12 MHz, meaning that $E$ region echoes are easily detected on low beam numbers.

In this paper we use data of echo power, Doppler velocity and spectral width obtained

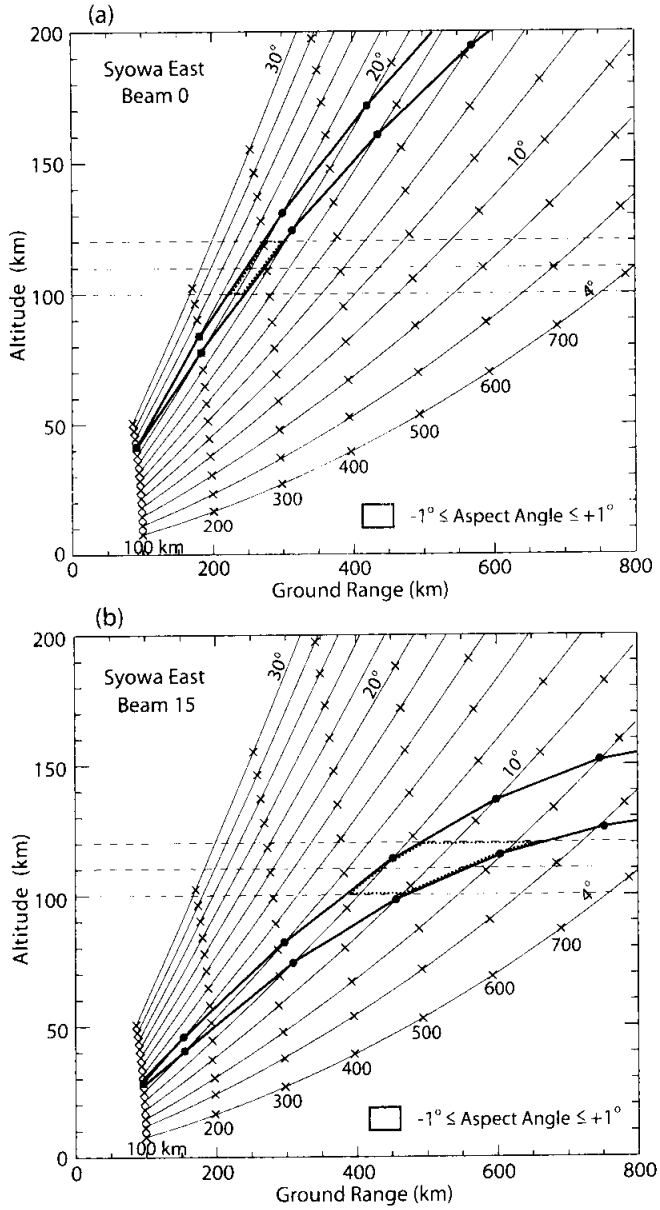


*Fig. 2. Ray paths with elevation angles of 4°-30° on (a) beam 0 and (b) beam 15 of the Syowa East radar in altitude-ground range coordinates. The area having $\alpha$ between $-1°$ and $+1°$ is surrounded by the thick solid curves. Slant ranges (100 km step) from Syowa Station are also indicated.*

by analyzing an auto-correlation function of radar echoes. In particular, the power and width were calculated by assuming an exponential fit to the auto-correlation function, which corresponds to a Lorentzian Doppler spectrum (*e.g.*, Hanuise *et al.*, 1993).

## 3. Observations

### *3.1. Weak disturbance (maximum $\Delta H \simeq +100$ nT)*

Figure 3 displays range-time variations of the echo power on beams 1, 7 and 14 on January 4, 1998 and the geomagnetic $H$ component (1-min average) observed with a magnetometer at Syowa on that day. The radar frequencies of 10.2–10.6 MHz were used for the observations. The $H$ component is rather quiet ($\Delta H \simeq 0$) before 1700 UT (UT $\simeq$ MLT and LT = UT + 3 hours at Syowa). At 1850 UT when $\Delta H$ increases to about +60 nT, the radar starts to detect echoes: the strongest echoes are located at slant ranges of around 270–360 km on beam 1, 315–405 km on beam 7 and 405–540 km on bean 14. Judging from Figs. 1 and 2, we conclude that these echoes are returned from the $E$ region altitudes of 100–120 km.

With gradually increasing $\Delta H$ due to the growing eastward electrojet, the echo ranges shift toward the radar. At 2015 UT when $\Delta H$ is most enhanced ($\simeq +100$ nT), the strongest echoes exist at 270–315 km on beams 1 and 7 and 315–405 km on beam 14, suggesting that the ray paths, in particular, for higher beam number, from the radar to echo targets in the $E$ region are not straight but refracted: we speculate from Fig. 2 that the rays with higher elevation angles are bent downward during propagation in the $D$ and lower $E$ region to satisfy the perpendicularity condition of $\alpha = 0°$ in the central $E$ region. With decreasing $\Delta H$ after 2015 UT, the echo ranges are unchangeable until 2120 UT, after which those on beams 7 and 14 tend to shift a little toward farther ranges. The echoes disappear at around 2135 UT when $\Delta H$ is +50 nT. Note that the echoes on beams 1 and 7 at ranges beyond 400 km after 1940 UT are backscattered from the $F$ region.

### *3.2. Strong disturbance (maximum $\Delta H \simeq -900$ nT)*

Range-time variations of the echo power on beams 1, 7 and 14 on January 6–7, 1998 are shown in Fig. 4. The radar frequencies varied between 10.2 and 11.5 MHz during the observations. Note that the radar operation was stopped between 1520 and 1600 UT and between 1630 and 1730 UT. The Syowa magnetogram indicates the following $\Delta H$ excursion: quiet before 1530 UT, almost positive (with a maximum of +200 nT at 1640 UT) until 0000 UT and negative (with a maximum of −900 nT at 0320 UT) until 0730 UT. The movement of the $E$ region echo ranges before 0000 UT is quite similar to the case shown in Section 3.1. The $F$ region echoes appear at ranges beyond 450 km. After 0000 UT, with increasing negative excursion of $\Delta H$ (caused by the growing westward electrojet), the echo ranges where the echo intensity has a maximum move toward the radar (the minimum ranges are 225–270 km on all the beams): this movement is larger on higher beam numbers. This fact suggests that the radar wave refraction is more severe for stronger disturbance and higher beam numbers (longer propagation distance).

To investigate in detail echo characteristics during this strong $\Delta H$ disturbance, Figs. 5a, 5b and 5c show range-time variation of the echo power, Doppler velocity (positive toward the radar) and spectral width, respectively, obtained on beam 14 for which the refraction effect is strongest. The $\Delta H$ variation is also displayed in the figure (Fig. 5d). Fig. 5a clearly demonstrates that between 0100 and 0630 UT when $\Delta H$ is disturbed, the strongest echoes appear at ranges of 225–405 km and moreover that the movement of the echo regions is in harmony with the $\Delta H$ variation, that is, the regions move toward (away

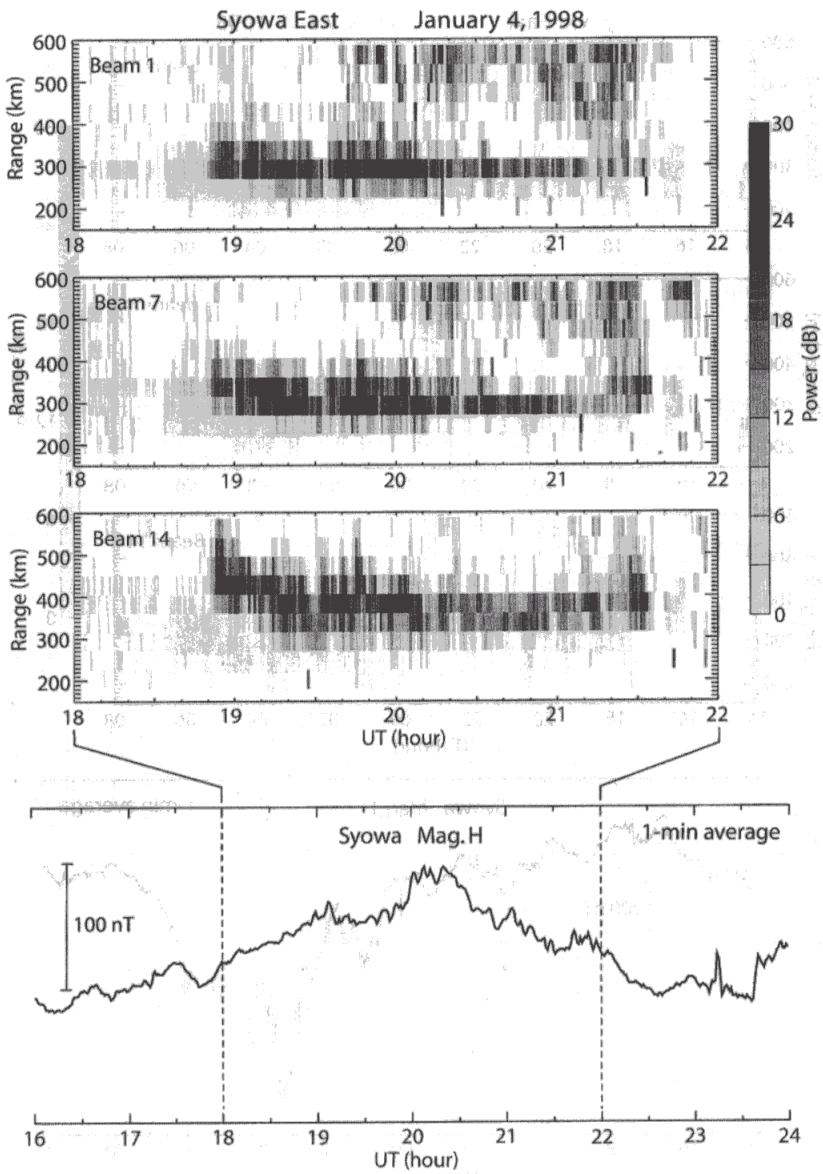


*Fig. 3. Slant range-time plots of echo power on beams 1, 7 and 14 and geomagnetic H component (1-min average) on January 4, 1998.*

from) the radar with increasing (decreasing) $\Delta H$.

The velocities (Fig. 5b) are positive ($\leq +400$ m/s) before 0100 UT and negative ($\leq -600$ m/s) after 0100 UT, corresponding to the westward electron drifts (eastward electrojet) and the eastward electron drifts (westward electrojet), respectively. The radar echo subsidence at around 0000 UT is caused by very weak electric fields (responsible for the irregularity production) near the Harang discontinuity. It is recognized that after 0100 UT

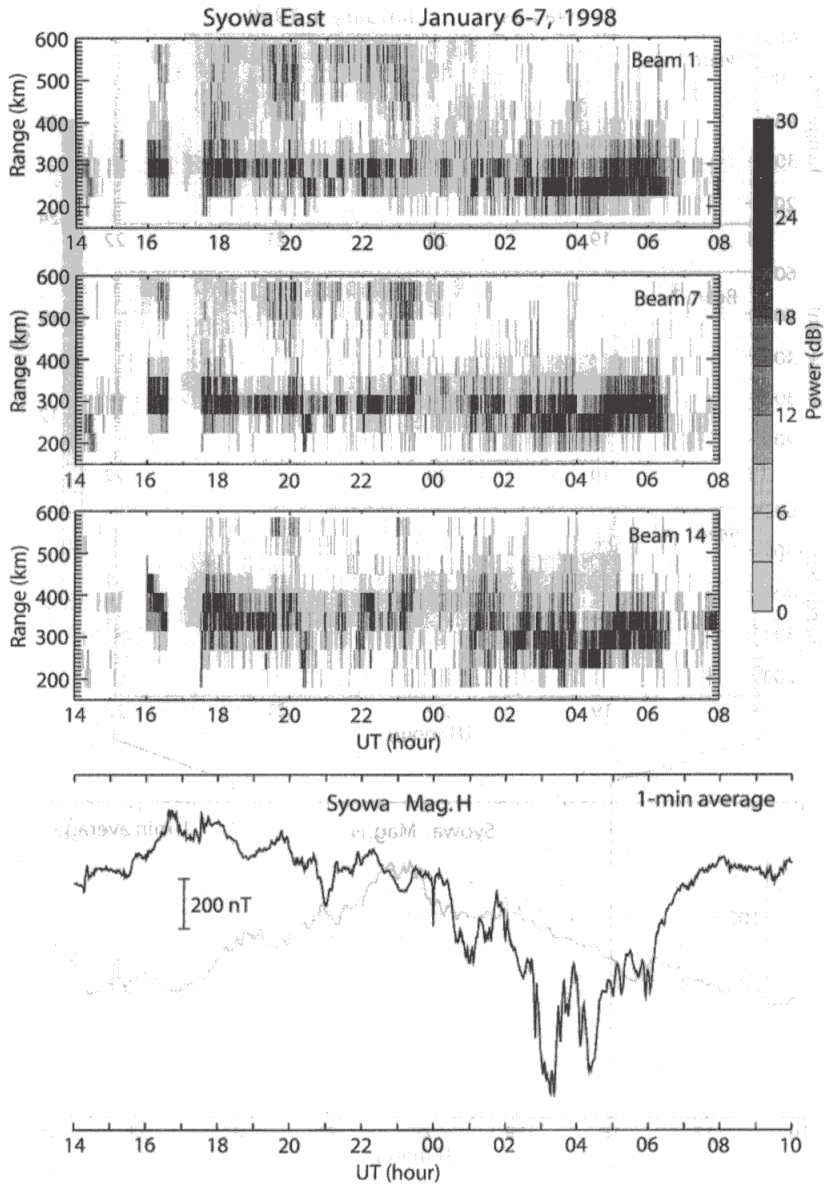


*Fig. 4. Same as Fig. 3 but for January 6–7, 1998. Note that the radar operation is stopped between 1520 and 1600 UT and between 1630 and 1730 UT.*

the velocity is faster for stronger echo intensity, a well-known fact for the *E* region irregularities (*e.g.*, Ogawa and Igarashi, 1982; Milan and Lester, 2001; Makarevitch *et al.*, 2001). The spectral width behavior (Fig. 5c) is interesting. The width after 0200 UT is narrower (wider) for stronger (weaker) echo intensity and faster (slower) velocity. These facts are clearly demonstrated in Fig. 6 in which time variations of the echo power, Doppler velocity and spectral width at the range gate of 270–315 km between 0420 and 0540 UT are

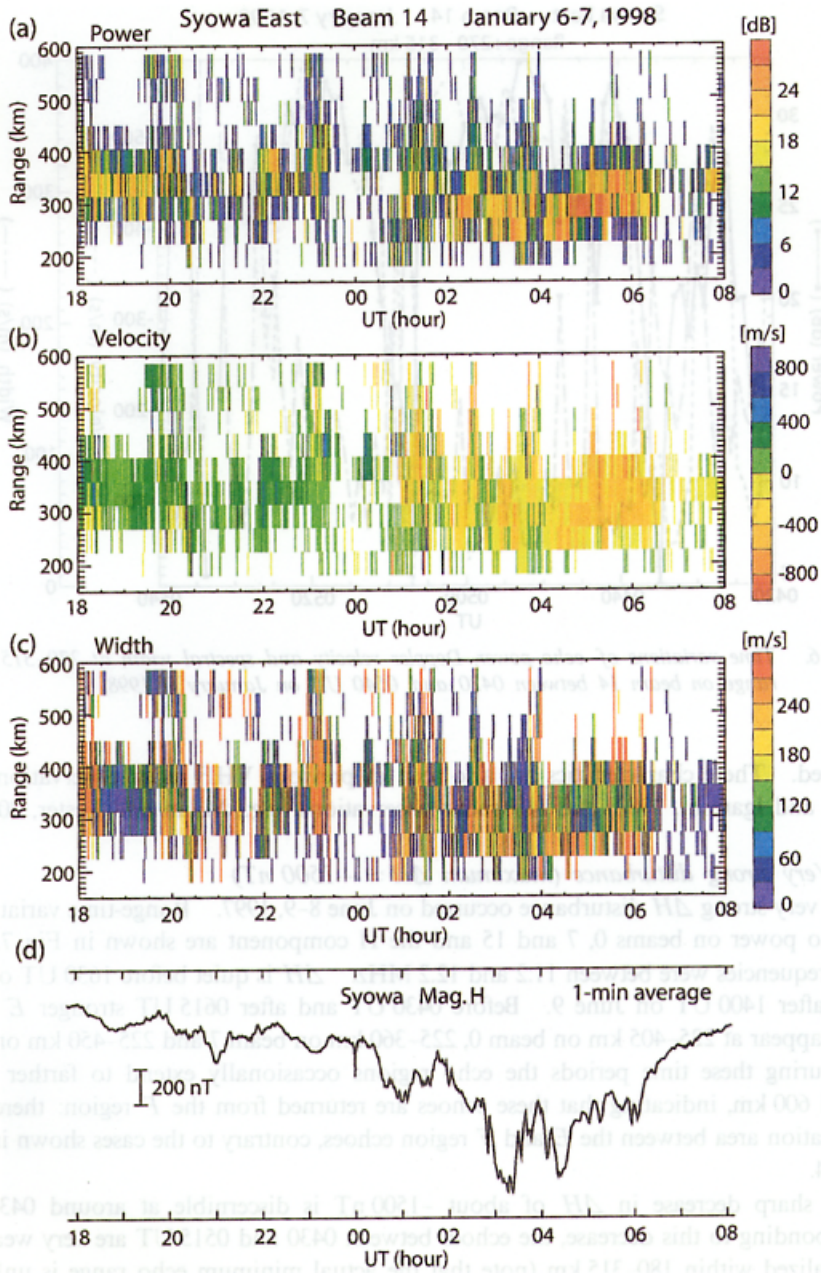


*Fig. 5. Slant range-time plots of (a) echo power, (b) Doppler velocity (positive toward the radar) and (c) spectral width on beam 14 and (d) geomagnetic H component (1-min average) on January 6-7, 1998.*

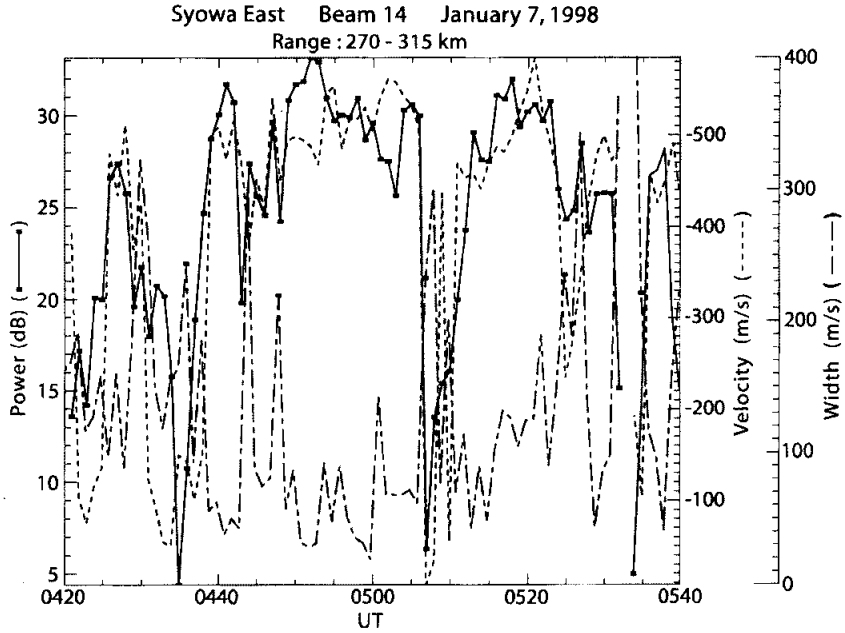


*Fig. 6. Time variations of echo power, Doppler velocity and spectral width at 270–315 km range on beam 14 between 0420 and 0540 UT on January 7, 1998.*

displayed. These characteristics are also seen in previous VHF radar observations (*e.g.*, Ogawa and Igarashi, 1982) and HF radar observations (*e.g.*, Milan and Lester, 2001).

### *3.3. Very strong disturbance (maximum $\Delta H \simeq -1500$ nT)*

A very strong $\Delta H$ disturbance occurred on June 8–9, 1997. Range-time variations of the echo power on beams 0, 7 and 15 and the H component are shown in Fig. 7. The radar frequencies were between 11.2 and 12.2 MHz. $\Delta H$ is quiet before 1630 UT on June 8 and after 1400 UT on June 9. Before 0430 UT and after 0615 UT stronger $E$ region echoes appear at 225–405 km on beam 0, 225–360 km on beam 7 and 225–450 km on beam 15. During these time periods the echo regions occasionally extend to farther ranges beyond 600 km, indicating that these echoes are returned from the $F$ region: there is no demarcation area between the $E$ and $F$ region echoes, contrary to the cases shown in Figs. 3 and 4.

A sharp decrease in $\Delta H$ of about −1500 nT is discernible at around 0430 UT. Corresponding to this decrease, the echoes between 0430 and 0515 UT are very weak and are localized within 180–315 km (note that the actual minimum echo range is unknown because of the first range gate of 180 km). Such features are not seen in Figs. 3 and 4. We speculate that largely enhanced $E$ and $D$ region electron density, due to high-energy particle precipitation associated with the strong substorms, caused complete absorption or forward reflection of the radar waves with lower elevation angles that would be backscattered at ranges beyond 315 km without the substorms.

Figure 8 shows range-time variations of the echo power (Fig. 8a), Doppler velocity

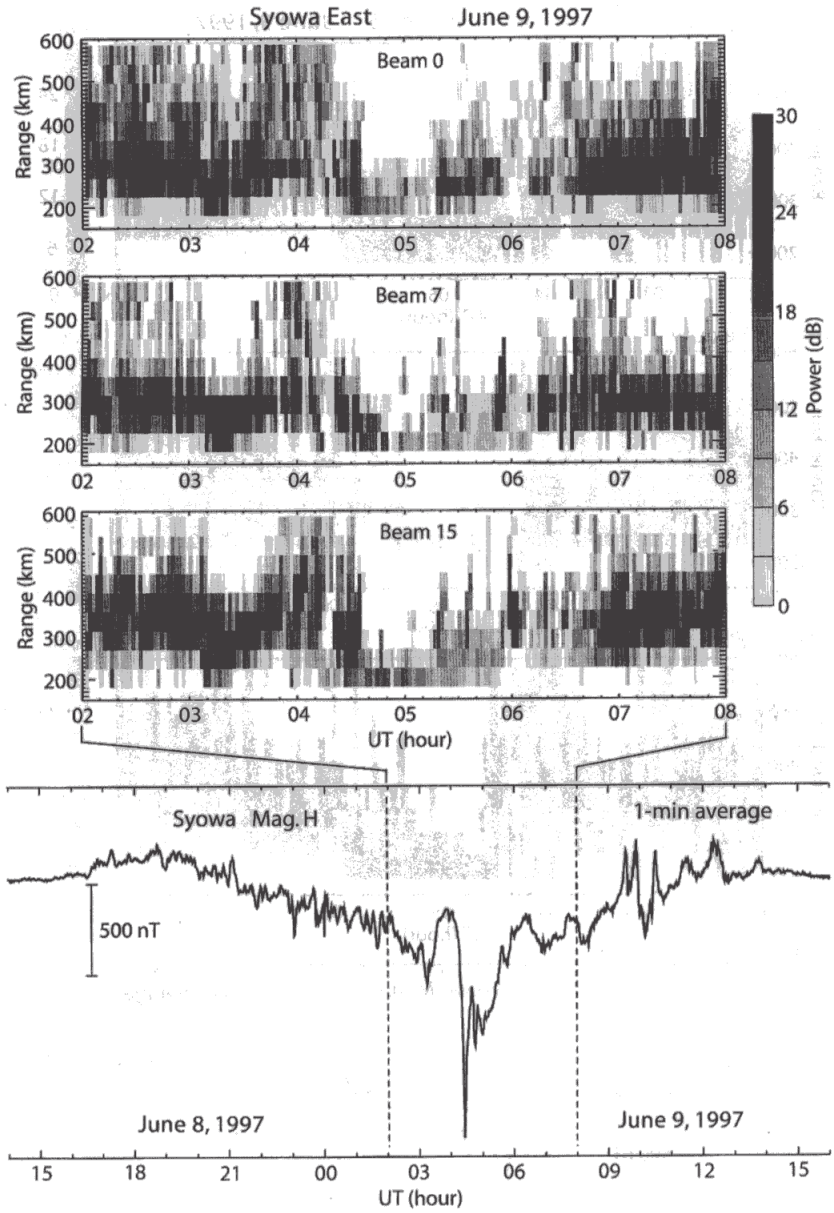


*Fig. 7. Same as Fig. 3 but for June 9, 1997.*

(Fig. 8b) and spectral width (Fig. 8c) on beam 15 together with the $H$ component (Fig. 8d). Between 0430 and 0515 UT the echo powers are less than 18 dB, most velocities are less than $-80$ m/s (note the maximum velocity of $-400$ m/s before 0430 and after 0515 UT) and the spectral widths at 180–225 km are less than 40 m/s. Such characteristics strongly suggest that the echoes are not returned form the central $E$ region but from the lower $E$ and $D$ regions. The echoes may partly include meteor echoes, usually occurring

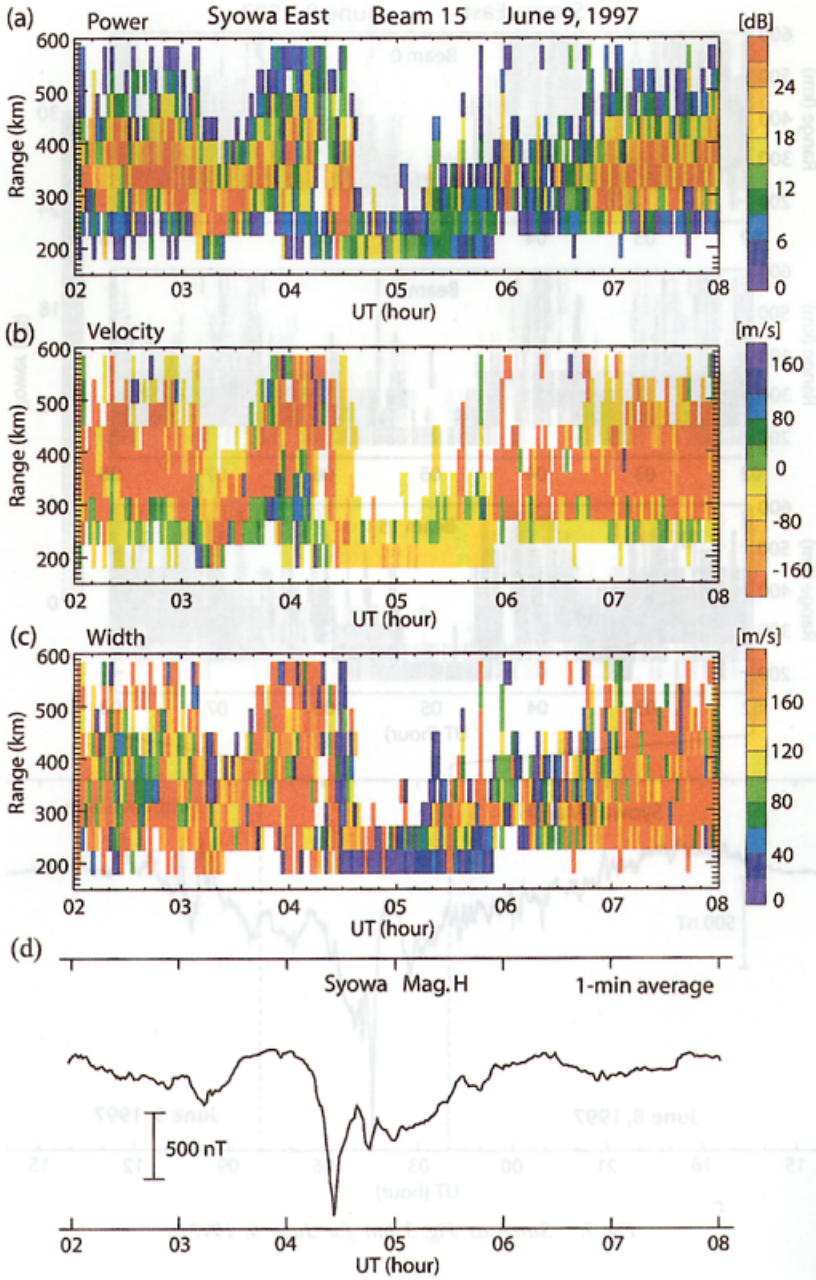


*Fig. 8. Same as Fig. 5 but for June 9, 1997.*

at 80–100 km altitudes, that have similar velocity and spectral width (Hall *et al.*, 1997). Note that the meteor echo occurrence at Syowa Station has a maximum at around 0300 UT (0600 LT) and a minimum at around 2000 UT (2300 LT) (Ogawa *et al.*, 1985).

## 4. Discussion

We have examined $E$ region echo characteristics under three kinds of geomagnetic disturbances, that is, weak disturbance (maximum $\Delta H \simeq +100$ nT), strong disturbance (maximum $\Delta H \simeq -900$ nT) and very strong disturbance (maximum $\Delta H \simeq -1500$ nT). The main results are as follows:

1) Under weakly disturbed conditions ($\Delta H \leq +100$ nT), strong echoes are returned from the central $E$ region. Radar wave refraction during propagation is negligible for lower beam numbers and a little more significant for higher beam numbers, that is, for longer propagation distance to the $E$ region.

2) Refraction effect becomes more pronounced with increasing $\Delta H$. Again, the refraction is most significant for higher beam numbers. Under a very strongly disturbed case (Fig. 7), echo ranges on all beams are limited to within 180 (first range gate)–315 km: in this case, as shown in Fig. 8, echo power, velocity and spectral width are all greatly reduced.

There are two kinds of plasma waves that produce field-aligned $E$ region irregularities. See papers by Haldoupis (1989), Ogawa *et al.* (2001) and references therein for more details of the $E$ region plasma instabilities. In the central $E$ region phase velocities of the gradient-drift (cross-field) waves are almost equal to $\mathbf{E}\times\mathbf{B}$ drift and those of the two-stream waves saturate at the local ion acoustic velocity. Below 100 km altitude the gradient-drift phase velocities are more reduced with decreasing altitude and the two-stream waves cannot be excited. Dimant and Sudan (1995) have proposed a new plasma instability that is probably operative below 90 km and has phase velocities less than 100 m/s. This instability, however, requires an electric field exceeding 50 mV/m ($\mathbf{E}\times\mathbf{B}$ drift of about 1000 m/s).

Relying on these considerations and current observations, Fig. 9 schematically illustrates simplified wave propagation modes (A, B and C) in the $E$ region under different disturbed conditions. In mode A for less disturbed condition, ray paths are almost straight, in particular, for low beam numbers, to achieve perpendicularity ($\alpha = 0^\circ$) in the central $E$ region. Mode B becomes dominant under disturbed condition and for higher beam numbers under weakly disturbed conditions; that is, the rays are refracted downward in the lower $E$ region (because of enhanced electron density) to achieve $\alpha \simeq 0^\circ$ in the central $E$ region. Propagation distance (radar range) in this mode should be shorter than that in mode A. In modes A and B, echo power, Doppler velocity and spectral width are not suppressed because the condition $\alpha = 0^\circ$ is satisfied in the central $E$ region.

In mode C for highly disturbed condition, rays are refracted in the $D$ and lower $E$ regions due to greatly enhanced electron density. The rays, however, cannot arrive at the central $E$ region and are backscattered from the lower $E$ region where $\alpha$'s is probably close to zero. As described above, below 100 km altitude the gradient-drift phase velocity deviates from $\mathbf{E}\times\mathbf{B}$ drift and decreases rapidly with decreasing altitude. In addition, we can expect that plasma turbulence below 100 km altitude is weaker than that in the central $E$ region, resulting in lower echo power and narrower spectral width below 100 km. The plasma instability proposed by Dimant and Sudan (1995) (see above) might be operative for our strongly disturbed case. Thus, mode C seems to well explain the above item 2: if echoes are returned from the central $E$ region (as in modes A and B), then echo power, Doppler velocity and spectral width are not reduced. Note that Doppler velocity is also

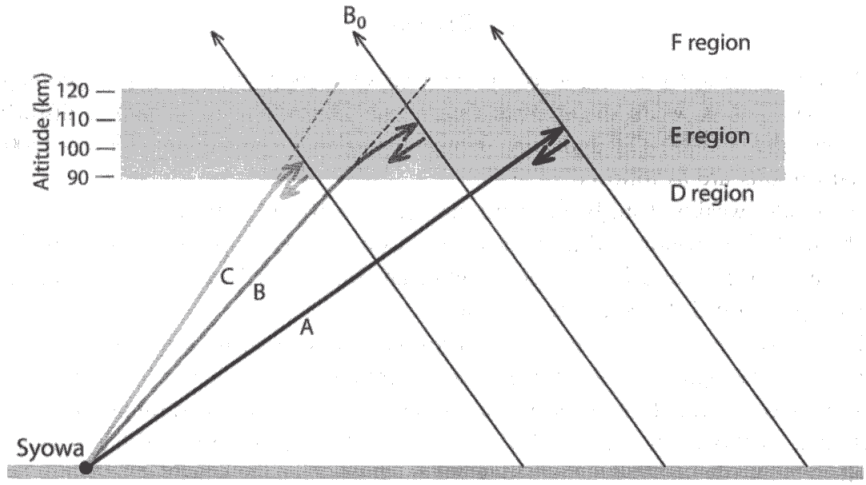


*Fig. 9. Schematic illustration of HF wave propagation mode in the E region under weakly (A), strongly (B) and very strongly (C) disturbed conditions.*

reduced when backscatter occurs at $\alpha \neq 0°$ in the central $E$ region (*e.g.*, Ogawa *et al.*, 1980, 1982; Fejer *et al.*, 1984).

The importance of wave refraction for the SuperDARN radars has been pointed out by Villain *et al.* (1984), Uspensky *et al.* (1994, 2001), Milan and Lester (1998), Koustov *et al.* (2001) and Makarevitch *et al.* (2001). This is confirmed by the current results. In our case, with increasing disturbance, the echo ranges become closer to the radar, meaning that ray paths should have higher elevation angles. Such an effect together with the vertical antenna patter of the radar must be taken into account in considering the echo power reduction at near-ranges.

For a target at a range of 180 km and an altitude of 100 km (Fig. 8), the elevation angle is 34° under no wave refraction. When a radio wave (frequency: $f$) enters an ionospheric plasma (plasma frequency: $f_p$) from below with an elevation angle of $\theta_i$, its path is bent downward to have an elevation angle of $\theta_r$. Snell's law tells that for $f = 11$ MHz and $\theta_i = 40°$, $\theta_r$ is 35°, 31°, 24° and 7° for $f_p = 4$, 5, 6 and 7 MHz, respectively. Thus, it seems easy that the wave vector becomes perpendicular to the geomagnetic field somewhere in the disturbed $E$ region.

Ogawa *et al.* (2001) speculated that low Doppler velocity ($\leq 100$ m/s) at short ranges (low altitudes) may be partly caused by neutral winds and/or turbulence of the neutral atmosphere. In addition, Ogawa *et al.* (2002) found that polar mesosphere summer echoes under quiet geomagnetic conditions have low velocity at ranges of 180–315 km. The present results suggest that the low velocity is also caused by field-aligned irregularities in the lower $E$ and $D$ regions under highly disturbed conditions.

## 5. Conclusions

Case studies of $E$ region HF radar echoes for a range of geomagnetic conditions have been presented. With increasing disturbance level, echo range becomes shorter because of

wave refraction during propagation due to more enhanced $D$ and $E$ region electron density. From analysis of power, Doppler velocity and spectral width of echoes, we have found that the echoes are returned from the central $E$ region, where $\alpha$ is close to zero, when geomagnetic disturbance is less than about $-900$ nT. When highly disturbed ($\simeq -1500$ nT), the echoes are returned from the $D$ and lower $E$ regions, resulting in suppression of echo power, Doppler velocity and spectral width. Our results suggest that we must always consider, more or less, the wave refraction effect in analyzing near-range HF radar echoes for the $E$ region study. In the future we need more sophisticated radar operation (shorter first-range gate and higher range resolution) to make more detailed investigations of refraction processes and scattering altitudes. HF ray-tracings using realistic electron density profiles in the $D$ and $E$ regions are necessary to know how the refraction is and where it occurs.

## Acknowledgments

We thank all the staff who contributed to the HF radar observations at Syowa Station. This research is supported by the Grant-in Aid for Scientific Research (A:11304029) from Japan Society for the Promotion of Science (JSPS). The Ministry of Education, Culture, Sports, Science and Technology supports the Syowa HF radar system.

The editor thanks Drs. T. Maruyama and M. Pinnock for their help in evaluating this paper.

## References

Dimant, Y.S. and Sudan, R.N. (1995): Kinetic theory of the Farley-Buneman instability in the $E$ region of the ionosphere. J. Geophys. Res., **100**, 14605–14623.

Fejer, B.G., Providakes, J. and Farley, D.T. (1984): Theory of plasma waves in the auroral $E$ region. J. Geophys. Res., **89**, 7487–7494.

Greenwald, R.A., Baker, K.B., Hutchins, R.A. and Hanuise, C. (1985): An HF phased-array radar for studying small-scale structure in the high-latitude ionosphere. Radio Sci., **20**, 63–79.

Greenwald, R.A., Baker, K.B., Dudeney, J.R., Pinnock, M., Jones, T.B., Thomas, E.C., Villain, J.-P., Cerisier, J.-C., Senior, C., Hanuise, C., Hunsucker, R.D., Sofko, G., Koehler, J., Nielsen, E., Pellinen, R., Walker, A.D.M., Sato, N. and Yamagishi, H. (1995): DARN/SuperDARN: A global view of the dynamics of high-latitude convection. Space Sci. Rev., **71**, 761–796.

Haldoupis, C. (1989): A review of radio studies of auroral $E$ region ionospheric irregularities. Ann. Geophys., **7**, 239–258.

Hall, G.E., MacDougall, J.W., Moorcroft, D.R., St.-Maurice, J.-P., Manson, A.H. and Meek, C.E. (1997): Super Dual Auroral Radar Network observations of meteor echoes. J. Geophys. Res., **102**, 14603–14614.

Hanuise, C., Villain, J.P., Gresillon, D., Cabrit, B., Greenwald, R.A. and Baker, K.B. (1993): Interpretation of HF radar ionospheric Doppler spectra by collective wave scattering theory. Ann. Geophys., **11**, 29–39.

Koustov, A.V., Igarashi, K., André, D., Ohtaka, K., Sato, N., Yamagishi, H. and Yukimatu, A.S. (2001): Observations of 50- and 12-MHz auroral coherent echoes at the Antarctic Syowa Station. J. Goephys. Res., **106**, 12875–12887.

Makarevitch, R.A., Ogawa, T., Igarashi, K., Koustov, A.V., Sato, N., Yamagishi, H. and Yukimatu, A. S. (2001): On the power-velocity relationship for 12- and 50-MHz auroral coherent echoes. J. Geophys. Res., **106**, 15455–15469.

Makarevitch, R.A., Koustov, A.V., Igarashi, K., Ohtaka, K., Ogawa, T., Nishitani, N., Sato, N., Yamagishi, H. and Yukimatu, A.S. (2002): Comparison of flow angle variations of $E$-region echo characteristics at VHF and HF. Adv. Polar Upper Atmos. Res., **16**, 59–83.

Milan, S.E. and Lester, M. (1998): Simultaneous observations at different altitudes of ionospheric backscatter in the eastward electrojet. Ann. Geophys., **16**, 55–68.

Milan, S.E. and Lester, M. (2001): A classification of spectral populations observed in HF radar backscatter from the $E$ region auroral electrojets. Ann. Geophys., **19**, 189–204.

Miyazaki, S., Ogawa, T. and Mori, H. (1981): Some features of nighttime $D$ and $E$ region electron density profiles in the polar ionosphere. Mem. Natl Inst. Polar Res., Spec. Issue, **18**, 304–311.

Ogawa, T. and Igarashi, K. (1982): VHF radar observation of auroral $E$-region irregularities associated with moving-arcs. Mem. Natl Inst. Polar Res., Spec. Issue, **22**, 125–139.

Ogawa, T., Mori, H. and Miyazaki, S. (1976): Rocket observations of electron density irregularities in the Antarctic auroral $E$ region. J. Geophys. Res., **81**, 4013–4015.

Ogawa, T., Balsley, B.B., Ecklund, W.L., Carter, D.A. and Johnston, P.E. (1980): Aspect angle dependence of irregularity phase velocities in the auroral electrojet. Geophys. Res. Lett., **7**, 1081–1084.

Ogawa, T., Balsley, B.B., Ecklund, W.L., Carter, D.A. and Johnston, P.E. (1982): Auroral radar observations at Siple Station, Antarctica. J. Atmos. Terr. Phys., **44**, 529–537.

Ogawa, T., Igarashi, K., Kuratani, Y., Fujii, R. and Hirasawa, T. (1985): Some initial results of 50 MHz meteor radar observation at Syowa Station. Mem. Natl Inst. Polar Res., Spec. Issue, **36**, 254–263.

Ogawa, T., Yamagishi, H., Ayukawa, I., Tanaka, T. and Igarashi, K. (1989): Simultaneous observations of radar aurora and visible aurora over Mizuho Station. Proc. NIPR Symp. Upper Atmos. Phys., **2**, 103–109.

Ogawa, T., Nishitani, N., Sato, N., Yamagishi, H. and Yukimatu, A.S. (2001): Implications of statistics of near-range Doppler velocity observed with the Syowa East HF radar. Adv. Polar Upper Atmos. Res., **15**, 82–102.

Ogawa, T., Nishitani, N., Sato, N., Yamagishi, H. and Yukimatu, A.S. (2002): Upper mesosphere summer echoes detected with the Antarctic Syowa HF radar. Geophys. Res. Lett., **29**(7), 10.1029/2001GL014094.

Uspensky, M.V., Kustov, A.V., Sofko, J.G., Koehler, J.A., Villain, J.P., Hanuise, C. Ruohoniemi, J.M. and Williams, P.J. (1994): Ionospheric refraction effects in slant range profiles of auroral HF coherent echoes. Radio Sci., **29**, 503–517.

Uspensky, M.V., Kustov, A.V., Eglitis, P., Huuskonen, A., Milan, S.E., Pulkkinen, T. and Pirjola, R. (2001): CUTLASS HF radar observations of high-velocity $E$-region echoes. Ann. Geophys., **19**, 411–424.

Villain, J.P., Greenwald, R. and Vickery, J.F. (1984): HF ray tracing at high latitudes using measured meridional electron density distributions. Radio Sci., **19**, 359–374.

*(Received January 24, 2002; Revised manuscript accepted June 6, 2002)*